Shear Deformation Kinematics During Cartilage Articulation: Effect of Lubrication, Degeneration, and Stress Relaxation

Benjamin L. Wong[*], **Won C. Bae**[*], **Kenneth R. Gratz**[*] **and Robert L. Sah**[*,†]

Abstract: During joint articulation, the biomechanical behavior of cartilage not only facilitates load-bearing and low-friction, but also provides regulatory cues to chondrocytes. Elucidation of cartilage kinematics under combined compression and shearing conditions clarifies these cues in health and disease. The objectives of this study were to elucidate the effects of lubricant, tissue degeneration, and stress relaxation duration on cartilage shear kinematics during articulation. Human osteochondral cores with normal and mildly degenerate surface structures were isolated. Paired blocks from each core were apposed, compressed, allowed to stress relax for 5 or 60 min, and shear tested with a micro-scale video microscopy system using phosphate-buffered saline (PBS) or synovial fluid as lubricant. During applied lateral motion, local and overall shear strain (E_{xz}) of articular cartilage were determined. The applied lateral displacement at which E_{xz} reached 50% of the peak ($\Delta x_{1/2}$) was also determined. Quantitatively, surface E_{xz} increased at the onset of lateral motion and peaked just as surfaces detached and slid. With continued lateral motion, surface E_{xz} was maintained. After short stress relaxation, effects of lubrication on E_{xz} and $\Delta x_{1/2}$ were not apparent. With prolonged stress relaxation, E_{xz} and $\Delta x_{1/2}$ near the articular surface increased markedly when PBS was used as lubricant. Similar patterns were observed for overall E_{xz} and $\Delta x_{1/2}$. With degeneration, surface E_{xz} was consistently higher for all cases after the onset of lateral motion. Thus, cartilage shear kinematics is markedly affected by lubricant, cartilage degeneration, and loading duration. Changes in these factors may be involved in the pathogenesis of osteoarthritis.

1 Introduction

Articular cartilage is a deformable, low-friction, and wear-resistant connective tissue that bears repeated loading and sliding during normal joint movement. After daily activities such as repeated knee bending (1) and running (2), overall cartilage thickness compresses ∼5-20%. The compression of cartilage at equilibrium is depth-varying, being highest near the articular surface and minimal in the deeper regions for dynamically compressed osteochondral blocks (3). Similarly, for compressed and sliding apposing osteochondral blocks, cartilage shear strain is highest near the articular surface and negligible near the tidemark, with cartilage shearing ∼2-5% overall after surfaces detached and slide (4). While recent investigations have elucidated the shear behavior of cartilage after achieving a steady state (i.e., after surfaces detach and slide), shear kinematics (i.e., prior to and after surface detachment and sliding) of cartilage articulation remains to be determined. Further characterization of apposing cartilage samples sliding relative to each other (Figure 1A,B) would further elicit the understanding of cartilage contact mechanics during joint loading by elucidating the changing boundary conditions at the articulating surface as well as the shear deformation of cartilage with applied lateral-loading, as opposed to after reaching a steady-state peak.

Lubrication of cartilage surfaces by pressurized interstitial fluid or boundary lubricants facilitate low friction during joint movement and may therefore affect the shear kinematics and sliding

---

[*] University of California–San Diego, La Jolla, CA.

[†] Correspondence author. Department of Bioengineering, Mail Code 0412, University of California–San Diego, 9500 Gilman Drive, La Jolla, CA 92093-0412. Tel: (858) 534-0821. Fax: (858) 822-1614. E-mail: rsah@ucsd.edu.
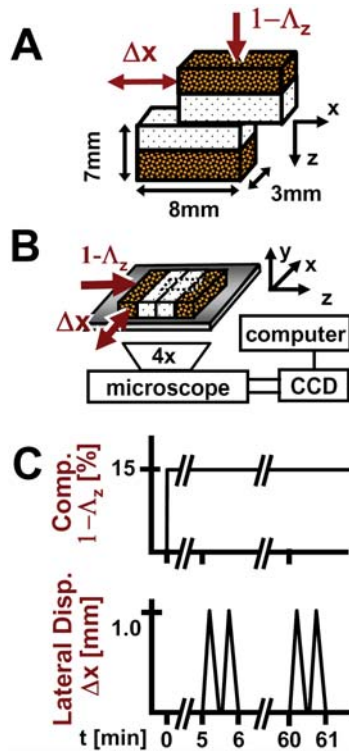
Figure 1: Schematics of (**A**) sample and testing configuration, (**B**) micro-shear test setup, and (**C**) loading protocol.

of articulating cartilage. At the onset of loading and/or motion, interstitial fluid within cartilage becomes pressurized and is forced between articulating surfaces to bear normal load and reduce interaction between contacting surfaces, facilitating low friction (5). After compression and stress relaxation to allow dissipation of hydrostatic pressure, the effects of boundary lubrication on articulating cartilage have been elucidated; synovial fluid (SF) and boundary lubricant molecules in SF reduce articular surface interaction as indicated by decreased friction (6, 7) and reduced surface shear strain (E_{xz}) (4). In contrast, the replacement of SF lubricant with phosphate buffered saline (PBS) results in an elevation of boundary-mode friction (6) and surface E_{xz} (4). Collectively, these studies suggest local and overall shear kinematics depends on both duration of loading (i.e., the time after onset and the extent of prolonged loading) and surface lubricant.

Cartilage degeneration may also affect shear de-

formation kinematics during joint movement. As cartilage undergoes degeneration, articular surfaces become fibrillated and roughened (8), which may lead to increased surface interaction between articulating cartilage surfaces. For articulating osteochondral blocks, peak cartilage E_{xz} near the surface increases with degeneration, while shear stiffness near the articular surface tends to decrease (4). While shear deformation increases with degeneration, whether increased friction or deteriorating shear properties are responsible for such changes in shear mechanics remain unclear. By characterizing shear kinematics during cartilage articulation for both normal and degenerate tissues, the mechanism by which degeneration increases shear deformation may be further elucidated.

Tracking of fiducial markers using a video microscopy system provides an approach to elucidate local and overall shear deformation and strain of cartilage during lateral-loading. Previously, a pair of osteochondral blocks were compressed in apposition and subjected to lateral shearing motion (Figure 1A) within physiologic range to mimic and study the biomechanical behavior of articulating cartilage at a micro-scale level after shear deformation reached a peak (4). Samples were allowed to stress relax for 1 hour to replicate deformation and strain that likely occurs after prolonged cyclic loading and sliding, rather than that which occurs at the onset of cyclic loading. However, with this configuration, shear deformation and strain can be captured during lateral-loading, as opposed to after reaching a peak. In addition, short stress-relaxation durations can be implemented to capture shear deformation that is likely representative of that occurring at the onset of cyclic loading. Thus, micro-scale analysis may be used to elucidate shear kinematics, locally and overall, during cartilage articulation near the onset of, or after prolonged, cyclic loading.

Thus, the governing hypothesis of this study was that the shear kinematics of cartilage during joint articulation is affected by lubrication, cartilage degeneration, and stress relaxation duration. The specific objective of this study was to determine the effects of (1) lubrication (PBS versus SF), (2)

degeneration (normal versus mildly degenerate), and (3) stress relaxation (5 min versus 60 min) on the shear deformation (tissue displacement) and shear strain (local and overall) of cartilage after compression and during applied lateral-loading in a cartilage-on-cartilage micro-scale shear test.

2 Methods

Sample Isolation: As previously described (4), 10 mm diameter osteochondral cores (n=6) were isolated, one each, from the anterior lateral femoral condyles of six fresh cadaveric human donors. Cores with grossly normal (NL, modified Outerbridge grade of 1 (9), n=3) or mildly degenerate (DGN; grade 3, n=3) surfaces were chosen from adult age groups of 41-60 yrs and >60 yrs, respectively. The cores were immersed in phosphate buffered saline (PBS) containing proteinase inhibitors (PI) and stored at -70°C until use.

On the day of testing, each core was thawed in PBS+PI and prepared for testing. The cartilage of each core was scored vertically using a razor blade, and the bone was cut using a low-speed saw with a 0.3 mm thick diamond edge blade (Isomet^{TM}, Buehler, Lake Bluff, IL) to yield two rectangular blocks for micro-scale shear testing (Figure 1A). Each of the two blocks had a cartilage surface area of $\sim 3 \times 8$ mm^2 and a total thickness of ~ 7 mm. From macroscopic images, thickness measurements were made at three separate locations and averaged to a yield a full cartilage thickness measurement for each sample.

Samples used in this study were characterized previously for histopathology (4), which confirmed the gross characterization of samples and the appropriate selection of NL and DGN samples for articulation testing. DGN samples exhibited structural (surface irregularity, vertical clefts to transitional zone, and transverse clefts) and cellular (cloning) features reflective of mild degeneration, while cellularity and glycoaminoglycan staining were normal and similar between NL and DGN samples.

Experimental Design: Micro-scale shear testing was conducted as previously described (4). First, samples were tested, as described below, with

PBS+PI as a lubricant. Then, samples were allowed to re-swell in PBS+PI for ~ 4 h at 4°C. Next, samples were tested again by micro-scale shear testing, this time with SF+PI as the lubricant. The SF was pooled from adult bovine knees, stored at -80°C, and characterized previously for boundary lubrication properties (6) and for levels of lubricant molecules (~ 1 mg/ml of hyaluronan and 0.45 mg/ml of proteoglycan 4 (10)). The same regions of interest were imaged and analyzed.

Micro-scale Shear Testing: Each sample consisted of paired osteochondral blocks and was mechanically tested as previously described (4). Samples were bathed for ~ 14-18 h in test lubricant containing PI and propidium iodide (20 μg/ml) to fluorescently highlight cell nuclei at 4°C prior to micro-shear testing.

Each pair of osteochondral blocks (Figure 1B) was then placed in a custom bi-axial loading chamber mounted onto an epi-fluorescence microscope for digital video imaging (11, 12) with cartilage surfaces in apposition. The bone of one block was secured while the apposing mobile block was allowed in-plane movement with orthogonally positioned plungers interfaced with either a micrometer (for axial displacement; Model 262RL; Starrett Co., Athol, MA) or motion-controller (for lateral displacement; Model MFN25PP; Newport, Irvine, CA). Fluorescence images (Nikon G-2A filter) with a field of view of $\sim 3 \times 2$ mm^2 were obtained at 5 frames/s, showing a full-thickness region of cartilage of the secured block and a partial-thickness region of cartilage of the apposing block.

Cartilage deformation was assessed similarly in the secured block during shear loading as previously described (4). An axial displacement was applied (~ 40 μm/s) by the micrometer to induce 15% compression (1-Λ_z, where Λ_z is the stretch ratio (13)) of the overall cartilage tissue thickness (Figure 1B,C). After 5 minutes of stress relaxation, lateral motion was applied to the mobile osteochondral block (Figure 1B,C). Two sets of lateral displacements (Δx), each consisting of +1 mm and then -1 mm (returning to initial position), were applied at 100 μm/s to the bone portion of

the mobile block. The first set, followed by a $\sim$12 s pause, was for preconditioning (6), while the second set was recorded for analysis. The sliding velocity was chosen based on the range of velocities (0-0.1 m/s) occurring during the loading (stance) phase of gait (14, 15). Subsequently, samples were then allowed to stress relax for a total of 60 min, and after, the two sets of lateral displacements were reapplied with shear deformation being recorded during the second set (Figure 1C). Experimentally, this duration of stress-relaxation was validated to be sufficient to reach a compressive equilibrium with load decreasing by 130 s to 50% of the peak, and load at one hour being only $3\pm1\%$ (n=3) higher than the load at 16 h. Before and during the application of lateral displacements (Figure 1B,C), sequential images, with $\sim$10 μm of lateral movement of the mobile block between frames, were taken to capture the shear deformation and sliding during cartilage articulation.

Data Analysis and Statistics: Digital micrographs were analyzed to determine the depth-varying and overall shear strains (E_{xz}) in cartilage as previously described (4) during cartilage articulation and lateral-loading. Briefly, images were analyzed in MATLAB 7.0 (Mathworks, Inc., Natick, MA) using image routines developed previously (16). First, an evenly distributed set of cell nuclei ($\sim$250 cell/mm^2), which served as fiducial markers, were selected and tracked by maximizing normalized cross-correlation of regions surrounding each marker to the preceding, and then initial frames. Local affine mappings of tracked nuclei at each captured frame were used to calculate the displacement of uniformly-spaced (10 pixels) mesh points in the region of interest ($\sim$1 mm $\times$ full thickness) during deformation. For each recorded image frame, displacement gradients were then determined by finite difference approximation, and in turn, used to determine Lagrangian shear strains (E_{xz}) after applied axial compression and during lateral shearing (17).

During applied lateral displacement (Δx), the calculated intra-tissue displacement (u) and shear strain (E_{xz}) were consolidated by first averaging and then interpolating values depth-wise. For each sample, u and E_{xz} at the same normalized depth (0, surface and 1, tidemark) were averaged and then interpolated linearly at every 5% of the normalized tissue thickness near the articular surface (i.e. 0 to 0.3) and 10% for remaining regions of the tissue depth (i.e. 0.3 to 1) after applied compression and during lateral motion. To consolidate data further, u and E_{xz} values were averaged among samples to yield an average depth-profile during applied lateral displacement.

From depth-averaged intra-tissue displacements and shear strains, u and E_{xz} near the articular surface, overall E_{xz}, and Δx at 50% peak surface and overall E_{xz} were determined and used for further comparisons. Surface E_{xz} and u were defined as that occurring at the top 5% of the cartilage thickness. The overall Lagrangian E_{xz} was determined as half *u* near the articular surface (u_s) normalized to the compressed cartilage thickness. Surface and overall E_{xz} and u_s were determined at Δx increments of 0.1 mm (Δx ranging between 0 to 0.8 mm) to assess the kinematics of cartilage shear deformation during articulation. To assess and compare rates at which surface and overall E_{xz} reached equilibrium, Δx when surface or overall E_{xz} reached 50% the peak value were determined for all experimental cases.

Data are reported as mean $\pm$ standard error of the mean (SEM), unless noted otherwise. Repeated measures ANOVA was used to determine the effects of stress relaxation (5, 60 min), applied lateral displacement (0-0.8 mm), lubricant (PBS, SF), and degeneration (NL, DGN) on tissue displacement and shear strain.

3 Results

Sample Characteristics: NL cores exhibited a glassy cartilage appearance with a smooth intact surface and had an average total tissue thickness of 1.86 ± 0.12 mm. Contrastingly, DGN cartilage appeared opaque with the surface being rough and fibrillated, and such samples had a slightly higher average tissue thickness of 2.08 ± 0.15 mm.

Cartilage Shear Deformation: As previously described (4), shear-loading resulted in a sequence of four events during cartilage articulation for all

cases. (1) Initially at the onset of Δx, cartilage surfaces adhered and began to displace (color map boundaries, Figure 2) laterally in unison, initiating E_{xz} (color map, Figure 2) near the articular surface (Figure 2A-D, I-II). (2) With increasing Δx, u and E_{xz} increased (Figure 2A-D, II). (3) Next, just as surfaces detached and slid relative to each another, cartilage u and E_{xz} peaked (Figure 2A-D, III). (4) With additional Δx, cartilage u and E_{xz} were maintained at steady-state peak (Figure 2A-D, IV). Effects of lubrication and degeneration on u_s (Figure 2A-D, i-iv) and E_{xz} (local and overall) were most apparent from these micrographs (Figure 2A-D, I-IV), and therefore, compared further.

Tissue displacement near the articular surface varied with Δx and was affected by degeneration, stress relaxation, and lubrication. With increasing Δx, magnitudes of u_s increased markedly (p<0.001), eventually reaching a maximum peak ranging from 50-125 μm and 120-170 μm for NL and DGN samples, respectively, for all experimental conditions (Figure 3). With degeneration, u_s was markedly higher (p<0.05) during lateral-loading for both test lubricants and stress relaxation durations. After a short 5 min stress relaxation period, differences due to lubrication in u_s were not apparent (Figure 3A) during shear-loading. While after 60 min of stress relaxation, u_s became significantly higher (interaction, p<0.05) when samples were tested in PBS than when tested with SF (Figure 3B) during applied lateral displacement (Δx) for both NL and DGN samples.

Cartilage E_{xz} during articulation varied with Δx and normalized tissue depth for both 5 and 60 min of stress relaxation. After 5 min of stress relaxation, E_{xz} was negligible throughout tissue depth when Δx is zero (Figure 4A). With increasing Δx, E_{xz} increased and became increasingly depth-varying (Figure 4B,C). At higher magnitudes of Δx, E_{xz} was highest near the articular surface and decreased monotonically with depth, becoming negligible near the tidemark (Figure 4D). Similar trends for cartilage E_{xz} were noted after 60 min of stress relaxation (Figure 4E-H). However, differences in depth-varying E_{xz} due to de-
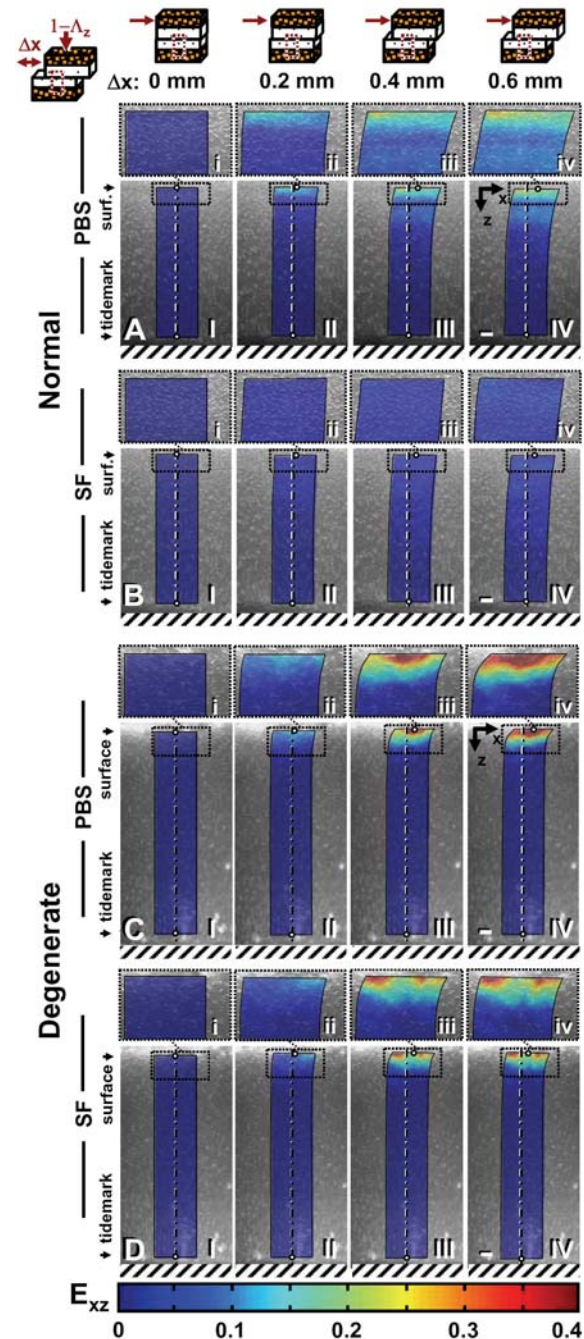

Figure 2: Micrographs taken during shear loading of apposing (**A,B**) normal and (**C,D**) degenerate samples lubricated with PBS (**A,C**) or SF (**B,D**) after 60 minutes of stress relaxation and (**I**) 0, (**II**) 0.2, (**III**) 0.4, and (**IV**) 0.6 mm of applied lateral displacement (Δx). Cell nuclei tracking method was used to determine (**I-IV**) maps of shear strain (color maps) with (**i-iv**) magnified views of the surface above. Bars = 150 μm.
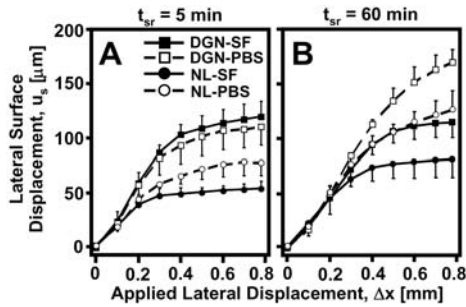
Figure 3: Lateral surface displacement (u_s) versus applied lateral displacement (Δx) for normal (NL: ●, ○) and degenerate (DGN: ■, □) cartilage after (**A**) 5 and (**B**) 60 minutes of stress relaxation time (t_{sr}). Samples were tested with phosphate buffered saline (PBS: ○, □) and synovial fluid (SF: ●, ■).
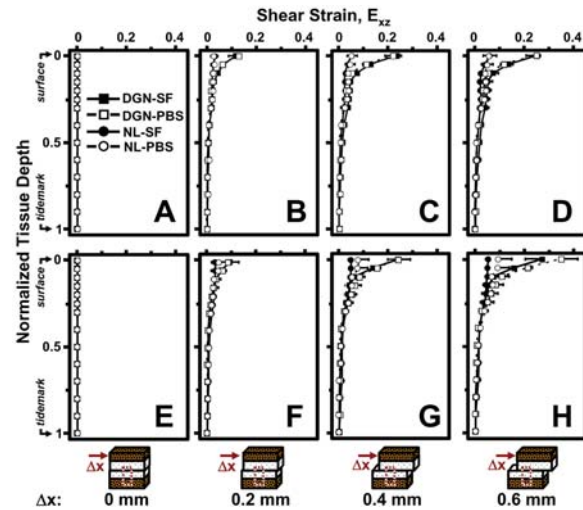

Figure 4: Local shear strain, E_{xz}, versus normalized tissue depth for normal (NL: ●, ○) and degenerate (DGN: ■, □) cartilage after 5 (**A-D**) and 60 (**E-H**) minutes of stress relaxation and (**A,E**) 0, (**B,F**) 0.2, (**C,G**) 0.4, and (**D,H**) 0.6 mm of applied lateral displacement (Δx). Samples were tested with phoshate buffered saline (PBS: ○, □) and synovial fluid (SF: ●, ■).

generation, lubrication, and stress relaxation became most apparent at higher magnitudes of applied lateral displacement.

Both surface and overall E_{xz} varied markedly with Δx and each was significantly affected by de-

generation, lubrication, and/or stress relaxation. Similarly to u_s, surface E_{xz} increased significantly (p<0.001) with Δx for all cases, eventually reaching a peak maximum (Figure 5A,B). During shear-loading, the E_{xz} near the articular surface for DGN samples was significantly higher (p<0.05) than NL samples for all lubricant (PBS, SF) and stress relaxation (5, 60 min) conditions. After 5 min of stress relaxation, differences in surface E_{xz} during lateral-loading due to lubrication were not apparent for both NL and DGN samples (Figure 5A). However, after 60 min of stress relaxation, surface E_{xz} during articulation was markedly higher when PBS was used as a lubricant than when SF was used, for both NL and DGN samples (interaction, p<0.001). Overall E_{xz} showed similar trends, increasing significantly with Δx (p<0.001) and when samples were tested with PBS as a lubricant and allowed to stress relax for 60 min (interaction, p<0.001) (Figure 5C,D). However, overall E_{xz} was not detectably different between NL and DGN samples during shear-loading (p=0.2) for all cases.
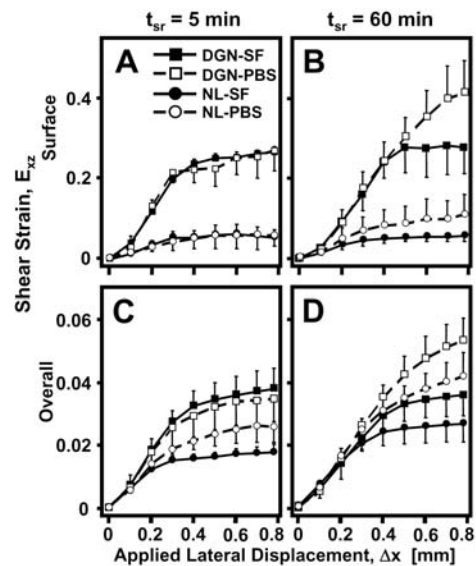

Figure 5: (**A,B**) Surface and (**C,D**) overall shear strain, E_{xz}, versus applied lateral displacement (Δx) for normal (NL: ●, ○) and degenerate (DGN: ■, □) cartilage after (**A,C**) 5 and (**B,D**) 60 minutes of stress relaxation time (t_{sr}). Samples were tested with phoshate buffered saline (PBS: ○, □) and synovial fluid (SF: ●, ■).

To assess the rate at which surface and overall E_{xz} reached their peaks during articulation, Δx at 50% peak E_{xz} ($\Delta x_{1/2}$) were determined and significantly varied with lubricant and stress relaxation. Differences in $\Delta x_{1/2}$ for surface (p=0.5) and overall (p=0.4) E_{xz} were not apparent between NL and DGN samples for all lubricant and stress relaxation conditions (Figure 6A-D). However, $\Delta x_{1/2}$ for surface E_{xz} markedly increased with PBS as lubricant in a stress-relaxation dependent manner (interaction, p<0.05). After 5 min of stress relaxation, surface $\Delta x_{1/2}$ was not detectably different (p=0.4) when samples were tested with PBS or SF as lubricant (Figure 6A). However after 60 min of stress relaxation, surface $\Delta x_{1/2}$ was 30-50% higher (p<0.01) with PBS than with SF as a lubricant (Figure 6B). Similar trends were also observed for overall $\Delta x_{1/2}$ (Figure 6C,D). When PBS lubricant was used, $\Delta x_{1/2}$ for overall E_{xz} was significantly higher than with SF in a stress-relaxation dependent-manner (interaction, p<0.01), being 25-40% greater (p<0.05) with PBS than SF after 60 min of stress relaxation (Figure 6D).

4 Discussion

This study elucidated the shear kinematics of cartilage-on-cartilage compression and sliding and suggests that four sequential events occur during cartilage-on-cartilage articulation (Figure 7). Initially when apposing cartilage layers are compressed against one another, adherence between articulating surfaces develops (Figure 7 A-I, B-I). With applied lateral displacement, the surfaces remain adhered; and as a result, the two cartilage layers behave as one contiguous tissue layer, and shear deformation increases in both cartilage layers (Figure 7 A-II, B-II). With continued applied lateral displacement, shear deformation continues to increase and eventually peaks just as the cartilage surfaces detach (Figure 7 A-III, B-III). With further applied lateral displacement, the articular surfaces slide across one another and peak shear deformation is maintained in both layers as the apposing cartilage layers undergo relative motion at the articular surfaces (Figure 7 A-IV, B-IV).

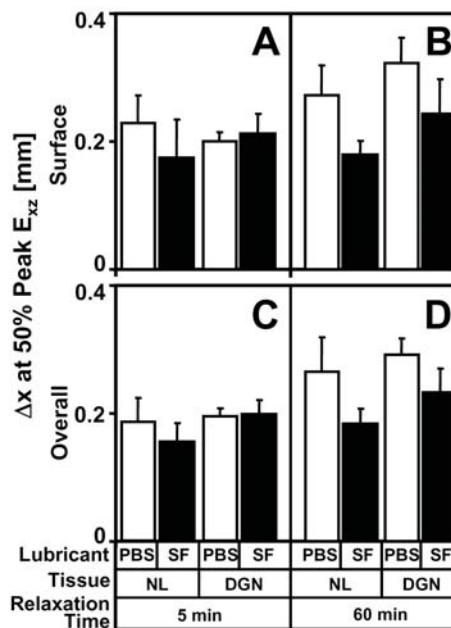The effects of lubrication, mild degeneration, and

Figure 6: Effect of lubricant (synovial fluid and PBS), degeneration (normal and degenerate), and stress relaxation time (5 and 60 minutes) on (**A**) surface and (**B** overall $\Delta x_{1/2}$ at 50% peak E_{xz} ($\Delta x_{1/2}$).
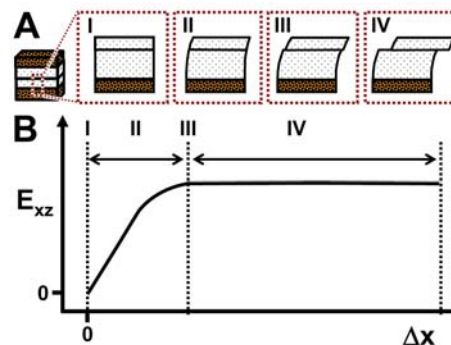
Figure 7: Four sequential events, (**I**) adherence, (**II**) adherence and shear deformation, (**III**) detachment as shear deformation peaks, and (**IV**) sliding with maintenance of shear deformation, that occurs during cartilage-on-cartilage articulation. (**A**) Schematic and (**B**) where these events occur in a representative shear strain (E_{xz}) versus applied lateral displacement (Δx) diagram.

stress relaxation on shear kinematics of cartilage-on-cartilage articulation were also found to be marked. With increasing Δx, u_s and E_{xz} in-

creased and peaked when surfaces began to slide, indicated by a plateau in E_{xz} despite increasing Δx (Figure 7B). The effect of lubrication was not apparent on shear deformation during lateral-loading after 5 min of stress relaxation (Figure 5A,C; 6A,C). However, after 60 min of stress relaxation, peak E_{xz} and $\Delta x_{1/2}$ increased with PBS as lubricant by ~100% and ~30-50%, respectively, near the surface (Figure 5B; 6B) and by ~55% and ~25-40%, respectively, overall (Figure 5D; 6D). When DGN samples were tested, E_{xz} near the surface was consistently higher than NL samples during lateral motion and was ~3-5 times higher at peak, being independent of stress relaxation duration and lubricant (Figure 5A,B).

The testing protocol used in this study mimics certain aspects of the compression and sliding of articular cartilage during normal joint loading. Cartilage within the knee undergoes a wide range of dynamic compression (5-20%) during normal activities (1, 2) and sliding up to ~50 mm (estimated from (14, 15)). The loading parameters used in this study mimic the high compressive loading and low sliding velocity events of gait, such as contralateral toe-off and heel rise (14). During such time, interaction of opposing articular surfaces is likely to be initiated and high. At the onset of cyclic loading, interstitial fluid within cartilage pressurizes and bears the majority of the load (5). After prolonged cyclic loading, cartilage gradually depressurizes and reaches an averaged steady-state compression (3). In this study, samples were allowed to stress-relax for both 5 and 60 minutes. As a result, the pattern of cartilage deformation and strain for short and prolonged stress-relaxation times are likely to be representative of that occurring near the onset and after prolonged cyclic loading, respectively.

The interactive effects of lubrication and stress relaxation time on cartilage shear kinematics is consistent with a transition in the dominating lubrication mode from interstitial fluid pressurization to boundary-mode during loading. Near the onset of compression, pressurized interstitial fluid between articular surfaces bears normal loads and offers little resistance to shear loads (5). As a result, cartilage E_{xz} will be low regardless of lubri-

cant near the onset of compression (Figure 5A,C). With prolonged compression, hydrostatic pressure of cartilage and the interstitial fluid between articular surfaces dissipates (18). At this point, direct surface-to-surface contact increases and bears a greater share of the normal load, and thus, resistance to shear loads becomes increasingly dependent on the presence/absence of boundary lubricants (19). Therefore, cartilage E_{xz} would be predicted to increase with the use of PBS, which is devoid of boundary lubricants, after prolonged compression, being consistent with the present results.

The reduction in E_{xz} with SF as lubricant after prolonged compression is consistent with predictions that account for past studies on cartilage boundary-mode friction. Synovial fluid decreases boundary-mode friction between articulating cartilage surfaces compared to saline (6, 7), and thus, reduces interaction between surfaces during articulation. As a result, cartilage surfaces would be predicted to slide at lower magnitudes of Δx with SF as lubricant than saline and result in a reduced peak tissue E_{xz}. After prolonged stress relaxation, $\Delta x_{1/2}$ was significantly lower for SF than PBS (Figure 6B,D), indicating tissue E_{xz} reached a peak sooner when SF was a lubricant. In addition, peak tissue E_{xz} was markedly decreased with SF at this time (Figure 5B,D). Collectively, such results suggest that surfaces slid sooner when SF was used as lubricant once hydrostatic pressure dissipated, which resulted in lowering tissue E_{xz}.

The increase in E_{xz} with degeneration, particularly near the articular surface (Figure 5A,B) with SF as a lubricant, is likely due to a reduction in tissue shear stiffness (modulus) and less likely due to an increase in cartilage friction. Magnitudes of E_{xz} near the articular surface were consistently greater in DGN than NL cartilage for each applied lateral displacement (Figure 5A,B). Such results would suggest a reduction in shear modulus near the articular surface, which agree with previously reported results (4), because shear modulus is estimated as an increment in shear load divided by an increment in E_{xz}. While roughened surfaces may lead to greater shear deformation by increasing surface interaction and thus friction, greater

shear with roughened surfaces may occur only if roughened surfaces slide at greater applied lateral loads than smooth surfaces. The present results indicate no apparent differences in $\Delta x_{1/2}$ between DGN and NL cartilage (Figure 6), suggesting DGN and NL cartilage slid at approximately the same point during lateral motion. Thus, friction was likely similar between the DGN and NL surfaces and did not contribute to increasing cartilage shear.

While the present results indicate the increase in shear deformation for DGN samples was due to a loss in shear stiffness, the cause (i.e., relative roles of friction and reduced shear modulus) of elevated shear with degeneration remains to be elucidated. Immediately following cartilage injury or wear, surface irregularities, such as chondral lesions, cracks, and focal defects, may result without any signs of fibrillation and apparent changes to the mechanical stiffness of cartilage. At this time, however, surface irregularities may increase roughness, and thus friction, causing surfaces to slide later than normal smooth surfaces which lead to elevated shear deformation. With continued loading over time (on the order of years), fibrillation may eventually develop that changes matrix structure and result in a decrease in mechanical stiffness and elevate shear deformation. Samples used in the present study were mildly degenerate, characterized by surface roughening and fibrillation, which likely is a result of years of loading following initial wear or injury. Thus, for DGN samples in this study, increased shear deformation was likely a result of decreased shear stiffness, while if DGN samples were taken immediately following injury or wear, elevated shear deformation would likely result from increased friction.

Collectively, this study provides insight into the effects of lubrication, degeneration, and stress relaxation on the shear kinematics of cartilage during joint articulation and its implications for cartilage degeneration. The present results suggest with prolonged loading, boundary lubricants modulate shear deformation by regulating when surfaces slide (sooner or later) during lateral motion. This is particularly important since

SF's boundary-lubricating function is markedly reduced in acute injury (20), which could cause surfaces to detach later during lateral movement and lead to elevated shear strain. In addition, degeneration results in increased shear strain despite normal SF lubricant function and duration of loading. Excessive magnitudes of compressive strain result in mechanical injury to cells (21, 22) and matrix (22, 23), which is likely similar for high E_{xz} magnitudes, predisposing cartilage to osteoarthritis and wear. Thus, development of treatments that not only restore mechanical integrity, but also restore SF lubricant function, may be critical in preventing shear-induced cartilage degradation and accelerated wear.

References

1. Eckstein F, Lemberger B, Stammberger T, Englmeier KH, Reiser M. 2000. Patellar cartilage deformation in vivo after static versus dynamic loading. *J Biomech*, 33(7):819-25.

2. Kersting UG, Stubendorff JJ, Schmidt MC, Bruggemann GP. 2005. Changes in knee cartilage volume and serum COMP concentration after running exercise. *Osteoarthritis Cartilage*, 13(10):925-34.

3. Neu CP, Hull ML, Walton JH. 2005. Heterogeneous three-dimensional strain fields during unconfined cyclic compression in bovine articular cartilage explants. *J Orthop Res*, 23(6):1390-8.

4. Wong BL, Bae WC, Chun J, Gratz KR, Sah RL. 2008. Biomechanics of Cartilage Articulation: Effects of Lubrication and Degeneration on Shear Deformation. *Arthritis Rheum*, In Press.

5. Ateshian GA, Mow VC. 2005. Friction, lubrication, and wear of articular cartilage and diarthrodial joints. In: Mow VC, Huiskes R,

editors. *Basic Orthopaedic Biomechanics and Mechano-Biology*. 3rd ed. Philadelphia: Lippincott Williams & Wilkins, p. 447-94.

6. Schmidt TA, Sah RL. 2007. Effect of synovial fluid on boundary lubrication of articular cartilage. *Osteoarthritis Cartilage*, 15:35-47.

7. Schmidt TA, Gastelum NS, Nguyen QT, Schumacher BL, Sah RL. 2007. Boundary lubrication of articular cartilage: role of synovial fluid constituents. *Arthritis Rheum*, 56:882-91.

8. Meachim G, Emery IH. 1974. Quantitative aspects of patello-femoral cartilage fibrillation in Liverpool necropsies. *Ann Rheum Dis*, 33:39-47.

9. Yamada K, Healey R, Amiel D, Lotz M, Coutts R. 2002. Subchondral bone of the human knee joint in aging and osteoarthritis. *Osteoarthritis Cartilage*, 10(5):360-9.

10. Mazzucco D, Scott R, Spector M. 2004. Composition of joint fluid in patients undergoing total knee replacement and revision arthroplasty: correlation with flow properties. *Biomaterials*, 25(18):4433-45.

11. Schinagl RM, Gurskis D, Chen AC, Sah RL. 1997. Depth-dependent confined compression modulus of full-thickness bovine articular cartilage. *J Orthop Res*, 15:499-506.

12. Chen SS, Falcovitz YH, Schneiderman R, Maroudas A, Sah RL. 2001. Depth-dependent compressive properties of normal aged human femoral head articular cartilage: relationship to fixed charge density. *Osteoarthritis Cartilage*, 9:561-9.

13. Fung YC. 1993. *Biomechanics: Mechanical Properties of Living Tissues*. 2nd ed. New York: Springer-Verlag.

14. Whittle M. 2002. *Gait analysis: an introduction*. 3rd ed. Oxford; Boston: Butterworth-Heinemann.

15. Shelburne KB, Torry MR, Pandy MG. 2005. Muscle, ligament, and joint-contact forces at the knee during walking. *Med Sci Sports Exerc*, 37(11):1948-56.

16. Gratz KR, Sah RL. 2008. Experimental measurement and quantification of frictional contact between biological surfaces experiencing large deformation and slip. *J Biomech*, 41:1333-40.

17. Fung YC. 1977. *A First Course in Continuum Mechanics*. 2nd ed. Englewood Cliffs: Prentice-Hall.

18. Krishnan R, Kopacz M, Ateshian GA. 2004. Experimental verification of the role of interstitial fluid pressurization in cartilage lubrication. *J Orthop Res*, 22(3):565-70.

19. McCutchen CW. 1966. Boundary lubrication by synovial fluid: demonstration and possible osmotic explanation. *Fed Proceedings*, 25:1061-68.

20. Elsaid KA, Jay GD, Warman ML, Rhee DK, Chichester CO. 2005. Association of articular cartilage degradation and loss of boundary-lubricating ability of synovial fluid following injury and inflammatory arthritis. *Arthritis Rheum*, 52(6):1746-55.

21. Loening A, Levenston M, James I, Nuttal M, Hung H, Gowen M, et al. 2000. Injurious mechanical compression of bovine articular cartilage induces chondrocyte apoptosis. *Arch Biochem Biophys*, 381:205-12.

22. Chen C-T, Bhargava M, Lin PM, Torzilli PA. 2003. Time, stress, and location dependent chondrocyte death and collagen damage in cyclically loaded articular cartilage. *J Orthop Res*, 21(5):888-98.

23. Thibault M, Poole AR, Buschmann MD. 2002. Cyclic compression of cartilage/bone explants in vitro leads to physical weakening, mechanical breakdown of collagen and release of matrix fragments. *J Orthop Res*, 20(6):1265-73.